TOC

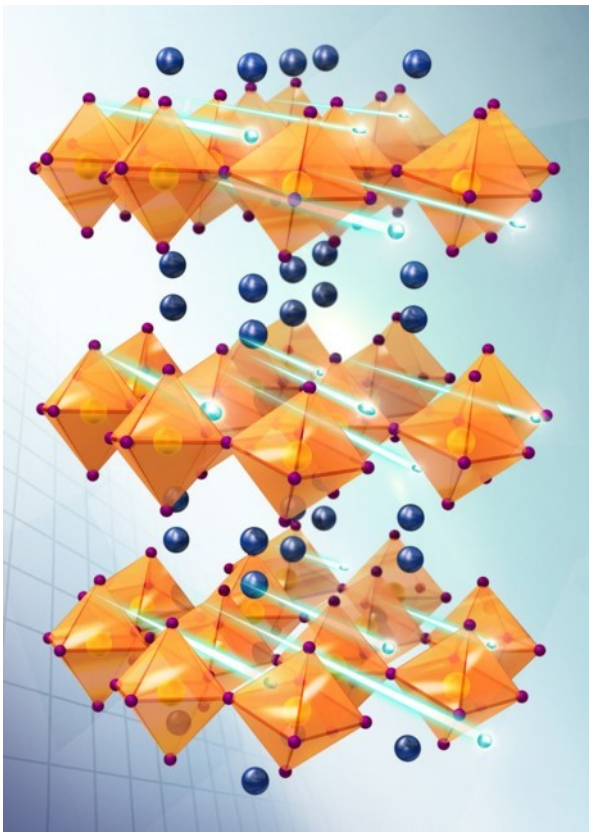

Extremely reduced dielectric confinement in two-dimensional hybrid perovskites with large polar organics

Ting-You Li[1†], Bin Cheng[1†], Partha Maity[2], Pai-Chun Wei[1], Dennis Nordlund[3], Kang-Ting Ho[1], Der-Hsien Lien[4], Chun-Ho Lin[1], Ru-Ze Liang[1], Xiaohe Miao[5], Idris A. Ajia[2], Jun Yin[2], Sokaras Dimosthenis[3], Ali Javey[4], Iman S. Roqan[2], Omar F. Mohammed[2], Jr-Hau He[1]*

[1]Computer, Electrical, and Mathematical Sciences and Engineering Division, King Abdullah University of Science and Technology (KAUST), Thuwal, 23955-6900, Kingdom of Saudi Arabia

[2]KAUST Solar Center, Physical Sciences and Engineering Division, King Abdullah University of Science and Technology (KAUST), Thuwal, 23955-6900, Kingdom of Saudi Arabia

[3]Stanford Synchrotron Radiation Lightsource, SLAC National Accelerator Laboratory, Menlo Park, CA 94025, USA.

[4]Electrical Engineering and Computer Sciences, University of California, Berkeley, CA 94720, USA

[5]Core Laboratories, King Abdullah University of Science and Technology, Thuwal, 23955-6900, Kingdom of Saudi Arabia

[†]These authors contributed equally to this work

[*]jrhau.he@kaust.edu.sa

Two dimensional (2D) inorganic-organic hybrid perovskites have recently attracted a substantial attention for photovoltaic application[1-6] due to their superior moisture stability compared to the conventional 3D perovskites structures. However, 2D perovskites suffer from not only quantum confinement, but also dielectric confinement which lead to large exciton binding energy

and low carrier mobility, and thus hinder their application perspective on the devices converting an optical input into current[1,2,5]. In this report, we theoretically predicted that extremely low exciton binding energy can be achieved by using high dielectric-constant organic groups, and demonstrated that in $(HOCH2CH2NH3)_2PbI_4$, whose organic groups have dielectric constant of 37, the dielectric confinement is largely reduced and thus an exciton binding energy of 13 meV has been obtained which is 20 times smaller than that in conventional 2D perovskites and also smaller than thermal activation energy at room temperature. As a result, the photo-induced excitons can be thermally dissociated efficiently at room temperature, as clearly indicated from femtosecond transient absorption (fs-TA) measurements. In addition, the mobility is largely improved due to the strong screening effect on charge impurities. Our low dielectric-confined 2D perovskites show excellent carrier extraction efficiency, and outstanding humidity resistance compared to conventional 2D perovskites.

Due to high absorption coefficient, intense photoluminescence, low electron-hole recombination rate and long carrier diffusion length, 3D perovskites are regarded as one of the leading candidates of next-generation photovoltaics (PVs) [7-10]. Recently, two dimensional layered organic-inorganic halide perovskites (2D perovskites) have been attracting attentions as an alternative to 3D perovskites in PV devices due to their improved stability and moisture resistance [1-3]. In addition, owing to the weak Van der Waals force between the functional organic groups, 2D perovskite nanosheets can be produced by solution method [4,5,11] and mechanical exfoliation [12] to fit limited geometric requirements, making them a new platform for low-dimensional nano-electronics/optoelectronics.

However, following the general trend of quantum confinement [13], the exciton binding energy of 2D perovskites is greatly increased compared to its 3D counterpart. Moreover, since the conventional organic linker used in 2D perovskites, such as $C_6H_5(CH_2)_2NH_3^+$ (PEA) and $C_4H_9NH_3^+$ (BA), have a small dielectric constant, the dielectric confinement emerges and makes the exciton binding energy even larger [13-16]. Such large exciton binding energy makes excitons difficult to form free carriers *via* thermal activation. Accordingly, the strong combined effect of quantum and dielectric confinement leads to carrier mobility in 2D perovskites two orders of magnitude lower than that in 3D perovskites [17]. In order to fully utilize the optoelectronic properties of 2D perovskites for photoelectric applications, intrinsic methods to lower the confinement in 2D perovskites are urgently required. Quantum confinement can be reduced by increasing the width of the inorganic semiconductor layer in 2D perovskites (see supplementary information), but even when the width of inorganic layer is enlarged by five times, the binding energy is still up to 200 meV [18]. Therefore, it is necessary to develop an alternative approach to “weaken” the dielectric confinement in 2D perovskites. However, the current method of reducing dielectric confinement by atom intercalation [19] can only lower the exciton binding energy by tens of meV, which is not enough for thermal dissociation of excitons at room temperature.

In this report, we conceived that by using large dielectric constant organic groups the dielectric confinement in 2D perovskite can be largely reduced. Then we demonstrated that $(HOCH_2CH_2NH_3)_2PbI_4$ (2D_EA perovskites) [20], in which the organic groups have dielectric constant of 37 [21] (Fig. 1a), has an twenty times smaller exciton binding energy and dozens of times larger carrier mobility compared to the high dielectric-confined 2D perovskites. It demonstrates that reducing dielectric confinement by using large dielectric constant organic groups is much more efficient than reducing quantum confinement and reducing dielectric confinement by atom

intercalation, leading to the significant improvement of carrier separation efficiency in 2D perovskites. Finally, we found that these low dielectric-confined 2D perovskites are highly stable under humidity, due to the strong dipole-dipole force between the organic groups.

First, for gaining the insight into the relations between exciton binding energy and dielectric constant of the organic layers in 2D perovskites, we adopted the image charge model [13]. According to our simulation (see supplementary materials), when the dielectric constant of organic layers is small, such as PEA whose dielectric constant is of ~3.3 [14] (Fig. 1b), Bohr radius describing the mean distance between the electron and hole in the exciton will decrease and accordingly the exciton binding energy will be largely enhanced (Fig. 1c), indicating a strong dielectric confinement. Conversely, as the dielectric constant of the organic layers increases, the dielectric screening effect will be enhanced, so that the Coulomb force between electron and hole in excitons will decrease, leading to increased Bohr radius and decreased exciton binding energy. If the dielectric constant of organic layer is sufficiently large, we can even achieve an exciton binding energy similar to that of 3D perovskites.

To experimentally achieve low dielectric-confined 2D perovskites, we used Ethanolamine (EA for a brief, and EA = $HOCH_2CH_2NH_3^+$) to form the organic layers (right inset of Fig. 1c). EA has a dielectric constant as high as 37, because of the charge dipole induced by hydroxy group and short carbon chain (Fig. 1a). The bulk single crystal of 2D_EA perovskite was confirmed by single crystal X-ray diffraction (XRD) (Table. S2). For comparison purpose, we also conducted measurements on $C_6H_5(CH_2)_2(NH_3)_2PbI_4$ (2D_PEA perovskites) single crystal (left inset of Fig. 1c), a conventional 2D perovskites widely used [1,5,11,22,23]. Temperature-dependent photoluminescence (PL) measurement was performed on both 2D_EA and 2D_PEA perovskites single crystals to determine the exciton binding energies. The PL intensity of 2D_EA perovskites drops rapidly as the temperature increases from 50 K to 160 K

(Fig. 2a), indicating weak attracting force between electron and hole induced by the screening effect (inset of Fig. 2a). Meanwhile the PL intensity of 2D_PEA perovskites shows a much slower decreasing rate as the temperature increases (Fig. 2b), indicating a more stable bound state for the excitons (inset of Fig. 2b). Integrated PL intensity was calculated (Fig. S1) and Arrhenius equation fitting (see supplementary materials) was used to get thermal dissociation ratio (Fig. 2c), obtaining a binding energy for 2D_EA perovskites of about 13 meV and for 2D_PEA perovskites about 250 meV. The absorption was taken on the micron-size flakes of those two 2D perovskites (see supplementary materials), and in 2D_PEA sample we can see the exciton peak while in 2D_EA sample the exciton peak is absent (Fig. 2d), indicating that the exciton binding energy in 2D_EA perovskite is much lower than that in 2D_PEA perovskite, which agrees with the temperature dependent measurement. Such exciton binding energy of the 2D_EA perovskites is as low as that of 3D perovskites, and one order-of-magnitude smaller than the lowest binding energy of conventional 2D perovskites reported [19], making thermally activated exciton dissociation to free carriers much more effective than that for conventional 2D perovskites [24].

To explore the exciton dissociation and free carrier generation processes in photoactive materials, different experimental and theoretical approaches can be employed. Femtosecond transient absorption spectroscopy (fs-TA) is one of the most robust and convenient choice [25,26]. To directly access to the free carrier generation and recombination, we have performed fs-TA measurements on those 2D perovskite crystals following 330-nm optical excitation. The experimental setup of the fs-TA is detailed elsewhere [27] (see also the supplementary materials). Fig. 3a and 3c show the TA spectra of 2D_EA and 2D_PEA perovskites, respectively following 330 nm excitation. As can be seen, in addition to the strong ground state bleaching (GSB) at 515 and 500 nm for 2D_EA and 2D_PEA perovskite, respectively, a broad excited-state absorption extending over the range of 530 to 750 nm. More

specifically, we notice a high intense photo induced absorption (PA) and low intense broad PA extended to the NIR region. The high and low PA signal can be attributed to as hot and free charge carriers, respectively. Interestingly, the broad photoinduced absorption intensity due to the free carrier is found to be three times higher for 2D_EA compared with 2D_PEA perovskite (Inset Fig. 3a, 3c); demonstrating the more efficient exciton dissociation in 2D_EA perovskite due to their lower exciton binding energy. The kinetics traces of GSB recovery and photoinduced absorption of both materials are shown in Fig. 3b and 3d. The dynamics of GSB recovery in 2D_EA perovskite shows two components, a fast 65.3 ± 4 ps and long 454.3 ± 26 ps. Similarly, the photoinduced absorption of 2D_EA perovskite shows two components of 66.8 ± 4.5 ps and 501.0 ± 28 ps. On the other hand, the GSB recovery and photoinduced absorption of 2D_PEA perovskite (Fig. 3d) show also two components of 7.4 ± 0.5 ps, 93 ± 6 ps and 8.1 ± 0.6 ps, 96 ± 6 ps, respectively. Being in this regime, it is well known that the carrier lifetime decreases (fast electron/hole recombination) as the exciton binding energy increases. In addition, the exciton dissociation and separation increase which lead to free carrier as the exciton binding energy decreases. To show the clear change in the TA data of 2D_EA and 2D_PEA, we have plotted the normalized bleach recovery kinetics and the excited state decay (Fig. S2) following 330 nm optical excitation. As can be seen from the kinetics traces that the GSB recovery and the excited state decay of EA is much slower than PEA, providing a clear experimental evidence for the lower exciton binding energy of the EA linked 2D perovskite. Slow GSB recovery and excited state decay results are consistent with our exciton binding energy results, and strongly prove 2D_EA perovskite has a longer carrier lifetime and more efficient exciton dissociation than 2D_PEA perovskite.

Carrier mobility is another important factor that affects the device performance of perovskites. In conventional 2D perovskites, the strong quantum confinement is known to be associated with the carrier mobility two

order-of-magnitude lower than that of 3D perovskites [17]. But it is rarely discussed that dielectric confinement is another important origin of such low mobility: a low dielectric constant of organic layer will reduce the screening effect of charge impurities, leading to a large scattering cross section and thus short relaxation time for charge carriers [28]. According to the Drude model, mobility $\mu = e\tau/m$ (τ is relaxation time of scattering, e is charge of one electron, and m is effective mass of carriers), short scattering relaxation time results in small mobility. Meanwhile, in 2D_EA perovskites, the time of flight measurement (TOF) shows that the carrier mobilities are about 11.1 and 9.5 $cm^2V^{-1}s^{-1}$ for electron and hole, respectively (Fig. 4a), and the Hall mobility determines an average value around 30 cm^2/Vs (hole mobility, see Supplementary Materials). The carrier mobilities in 2D_EA perovskites demonstrated here are much larger than those reported in conventional 2D perovskites [17,22]. According to the Density Functional Theory (DFT) based band structure calculations (Fig. S3), the effective mass of carriers in 2D_EA perovskites is similar to that in conventional 2D perovskites (Table. S1), so we attribute the improved mobility in 2D_EA perovskites to the increased relaxation time caused by enhanced screening effect resulting from the high dielectric constant of the organic layers [28].

Thanks to low binding energy and high carrier mobility, 2D_EA perovskites are expected to present much better photo-excited carrier extraction efficiency compared to conventional 2D perovskites in terms of responsivity, photo gain, and response time. As shown in Fig. 4b, in the metal-semiconductor-metal (MSM) structure based on 2D-EA perovskites, we achieve ~10 times higher photoresponsivity than that 2D_PEA over a wide range of incident light wavelength from 360 nm to 600 nm (Fig. 4b). As shown in Fig. 4c, the photo gain of 2D_EA perovskites is also one order-of-magnitude higher than that of 2D_PEA perovskites (we chose incident light wavelength 550 nm for 2D_EA perovskites, and 530 nm for 2D_PEA perovskites to achieve their best photo gain, respectively). Note that the

MSM junctions were done within one hour in vacuum after the perovskite crystal was prepared and we finished the measurement in two hours. Basically, the photo gain is proportional to τ_1/τ_t, where τ_1 and τ_t are carrier lifetime and carrier transit time, respectively [29]. τ_1 in 2D_EA perovskites is large because excitons are easily dissociated to free carriers, which reduces the probability of recombination. τ_t is defined by $d^2/V\mu$, where d is the distance between two electrodes (20 um for both 2D_EA and 2D_PEA perovskite MSM junction), V is the applied bias voltage, and μ is the carrier mobility. It is found that longer carrier lifetime and larger carrier mobility in 2D_EA perovskites result in a much larger photo gain than that in 2D_PEA MSM junction. Photoelectric response time is another critical parameter for evaluating the photo-excited carrier extraction efficiency. We selected 3V for bias voltage because 3V is larger than the saturation voltage (Fig. 4c), and got 53.4 us of the rising time and 57.2 us of the decay time in 2D_EA (Fig. 4d), which is ~2 order-of-magnitude shorter than that of 2D_PEA (3.78 ms and 4.30 ms for rising and decay time as shown in inset of Fig. 4d). Generally, the response time is proportional to the carrier transit time in semiconductor and photo-excited carrier transfer time in semiconductor/metal interface. Carrier transit time is inversely proportional to the carrier mobility [30], which is only about ~1 order-of-magnitude different in those two perovskites. As a result, the photo-excited carrier extraction time in 2D_EA perovskite/metal interface is much faster than that in 2D_PEA perovskite/metal interface. Here, based on the results of responsivity, photo gain, and response time we conclude that due to low binding energy and high carrier mobility 2D_EA perovskite show the signficantly improved carrier extraction efficiency, which is expected to have huge impact on the optoelectronic devies particularly for solar cells and photodetectors. For implementing 2D_EA perovskite in the devices, more device fabrication optimization is further needed and under investigation.

Our method of reducing dielectric constant in 2D perovskites can be generalized in several aspects. For example, if the halogen I is replaced by Br to synthesize EA_2PbBr_4, a similarly low exciton binding energy can be achieved (Fig. S4). As shown in Fig. S5, the ratio of I and Br can even be tuned to achieve color-tuning photoluminescence. Furthermore, as discussed earlier, the dielectric confinement reduction by inserting high dielectric-constant organic layers can combine with quantum confinement reduction by increasing the thickness of inorganic PbI layer in 2D_EA perovskites for achieving further decrease in exciton binding energy and increase in mobility [17,28].

In addition to optoelectronic properties, stability under humidity is crucial metric for PVs and one of the major obstacles for commercial adoption of perovskite PV technologies [1,2]. A variety of technological methods have been proposed to address the instability problem, including “intrinsic” method adopting the hydrophobic properties of organic group for preventing the perovskite framework from the direct exposure to moisture, and “extrinsic” method done by the encapsulated technic where the polycrystalline thin film can be protected by transportation layers [2]. In this report, we focus on single crystals without any transportation layer so that we can get insight into the “intrinsic” humidity stability related to the organic groups only. 2D_EA and 2D_PEA perovskite single crystals were exposed to an environment of 60% Relative humidity (RH) and 20 ^{o}C temperature, and time-dependent photo-responsivity of MSM junction based on those crytals were measured. As shown in Fig. 5b, photoresponsivity of 2D_PEA MSM junction started to decrease in a few hours (*e.x.* a 30% decrease after 48 hours). The 2D_EA MSM junction show a much better stability and remain at ~90% photoresponsivity after five days relative to its starting value. Our results indicate that 2D_EA perovskites can lead to a much better humidity resistance than conventional 2D perovskites.

To prove the enhanced humidity stability of 2D_EA single crystal, time-dependent XRD (TDXRD) was measured. The TDXRD of 2D_EA single crystal does not show any indication of degradation after 20 days exposed in 60% RH, 20 ^{o}C environment. On the other hand, the TDXRD of 2D_PEA shows a new peak which can be attribed to PbI_2 only after one day exposed in 60% RH, 20 ^{o}C environment (Fig. S6). To gain further insight into the excellent stability of 2D_EA perovskites, time-dependent X-ray photoelectron spectroscopy (XPS) of the Pb4f region was measured on 2D_EA single crystals to test the degradation as a function of exposure time in 60% RH, 20 ^{o}C environment. In Fig. S7, the peaks at 137.9 eV and 142.5 eV, corresponding to the binding energy of Pb $4f_{7/2}$ and Pb $4f_{5/2}$ of Pb-I in 2D_EA single crystal, do not show any indication of degradation after six days. To evaluate the chemical composition of the surface, we recorded XPS at 360 eV incidence photon energy, corresponding to a mean free path (for the outgoing ~220 eV photoelectrons) of less than 1 nm. 2D_EA perovskites (Fig. S8) was unchanged over six days without any indication of a PbI_2 or Pb^0 peak [31]. These XRD and XPS results confirmed the outstanding humidity stability of 2D_EA perovskites as shown in time-dependent photoresponsivity results. We attribute the remarkable enhancement of stability in 2D_EA perovskites to the strong hydrogen bonding between the organic layers (Fig. 5a) compared to that in 2D_PEA crystal (London dispersion force), so that our hydrophilic organic groups can restrict the penetration of water and oxygen more effectively.

In summary, the effect of organic layer with different dielectric constant on the exciton binding energy and carrier mobility in 2D perovskites was investigated. We found that the dielectric confinement effect can be significantly tuned by inserting different dielectric-constant organic layers between inorganic Pb-I units. To investigate this concept, we compared two different kind of 2D perovksite, one is highly dielectric-confined and the other one has a extremely low dielectric confinement, showing that in the

low-dielectric-confined 2D perovskites the exciton binding energy is of ~13 meV which is twenty times smaller than that in high dielectric-confined 2D perovskites. Moreover, in the low-dielectric-confined 2D perovskite single crystal we demonstrated excellent photo-excited carrier extraction efficiency due to largely improved carrier mobility and exciton binding energy, and moisture-resistance. The low dielectric-confined 2D perovskites might provide an alternative way to upgrade hybrid perovskite optoelectronics.

Figure Captions

Figure 1| **Exciton binding energy and Bohr radius.** Schematic diagram of **a,** EA molecule and **b,** PEA molecule. Large charge dipole caused by O-H bond is illuminated in EA. **c,** Exciton binding energy and Bohr radius as a function of organic-group dielectric constant in 2D perovskites predicted by image charge model. Calculated exciton binding energies and Bohr radii of PEA (square) and EA (diamond) based 2D perovskites are indicated. **Inset:** Lattice structures of 2D_EA perovskites (**right**) and 2D_PEA perovskites (**left**)

Figure 2| **Optical properties.** Temperature-dependent PL of **a,** 2D_EA and **b,** 2D_PEA perovskite single crystals. **c**, Exciton dissociation rate extracted from temperature dependent PLQE in both 2D_EA and 2D_PEA perovskites. **d,** Absorption of 2D_EA and 2D_PEA perovskites.

Figure 3| **Charge carrier dynamics.** fs-TA spectra at different time delay following 330 nm laser excitation of **a,** 2D_EA and **c,** 2D_PEA perovskites. Inset shows magnifying TA spectra in 550 to 750 nm spectral range. Kinetics traces of **b,** 2D_EA and **d,** 2D_PEA perovskite monitored at GSB maxima (red, 515 and 500 nm) and at 740 nm (blue), respectively. The amplitude of the TA signals of both cases are rescaled with respect to GSB intensity.

Figure 4|**Optoelectronic properties and carrier transport. a,** Linear fit of transit time versus inverse voltage V^{-1} of 2D_EA perovskites in Time of Flight measurements. **b,** Wavelength-dependent photoresponsivity of 2D_EA and 2D_PEA perovskites under 10 W/m^2 power density at 3 V bias voltage. **c,** Photogain of 2D_EA and 2D_PEA and under 5 W/m^2 power density at 550 and 530 nm light, respectively. **d,** Transient photoresponse of 2D_EA and 2D_PEA (**inset**) single crystal perovskites under 5 W/m^2 power density at 550 and 530 nm light, respectively.

Figure 5|**Humidity stability. a,** Normalized time dependent responsivity of 2D_EA and 2D_PEA perovskites. **b,** Schematic diagram of hydrogen bonds between the organic layers in 2D_EA perovskites.

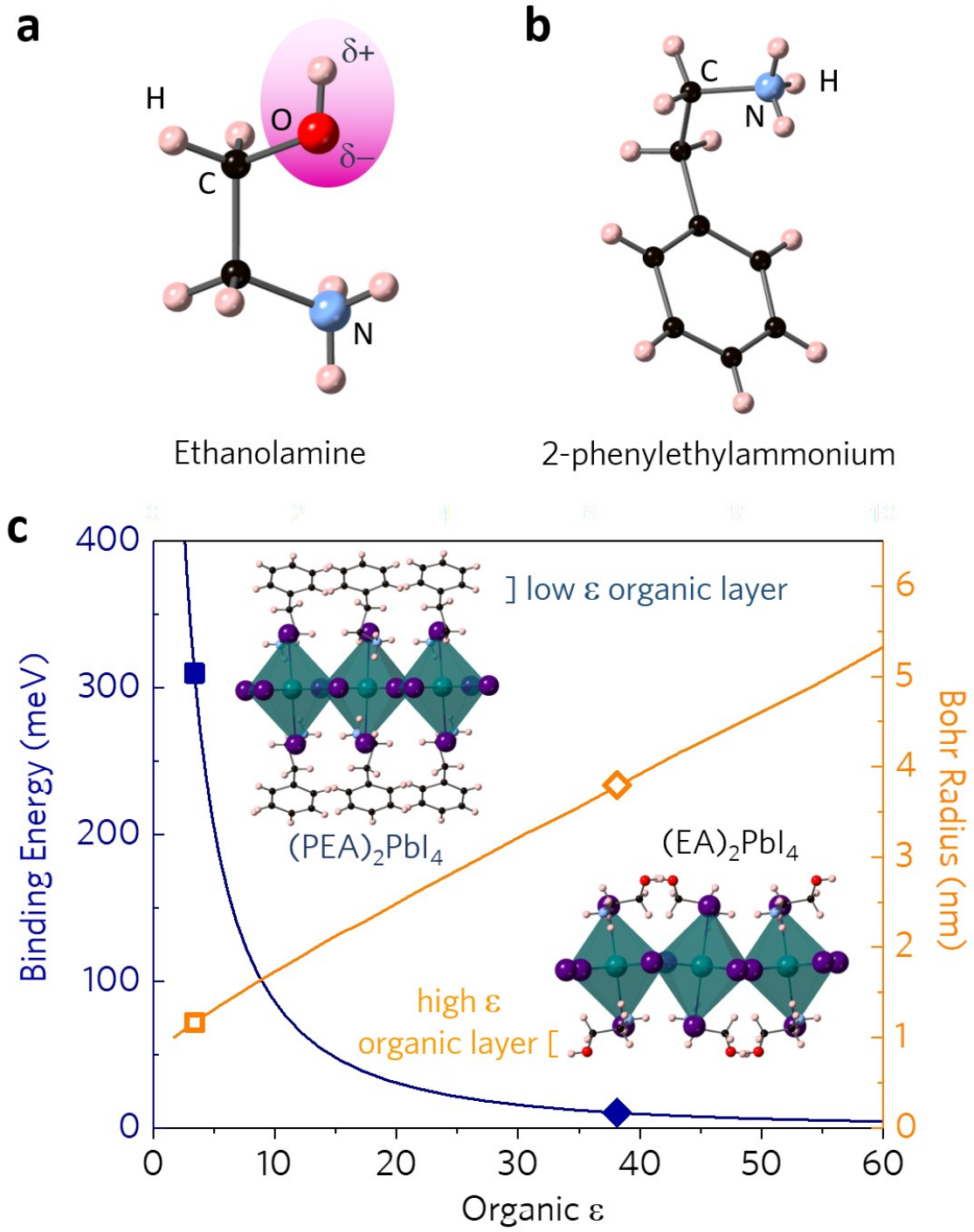
a
δ+
H
O
δ–
C
N
Ethanolamine
b
C
H
N
2-phenylethylammonium
c
400
300
200
100
0
Binding Energy (meV)
0
10
20
30
40
50
60
Organic ε
6
5
4
3
2
1
0
Bohr Radius (nm)
] low ε organic layer
(PEA)2PbI4
(EA)2PbI4
high ε
organic layer [

Figure 1

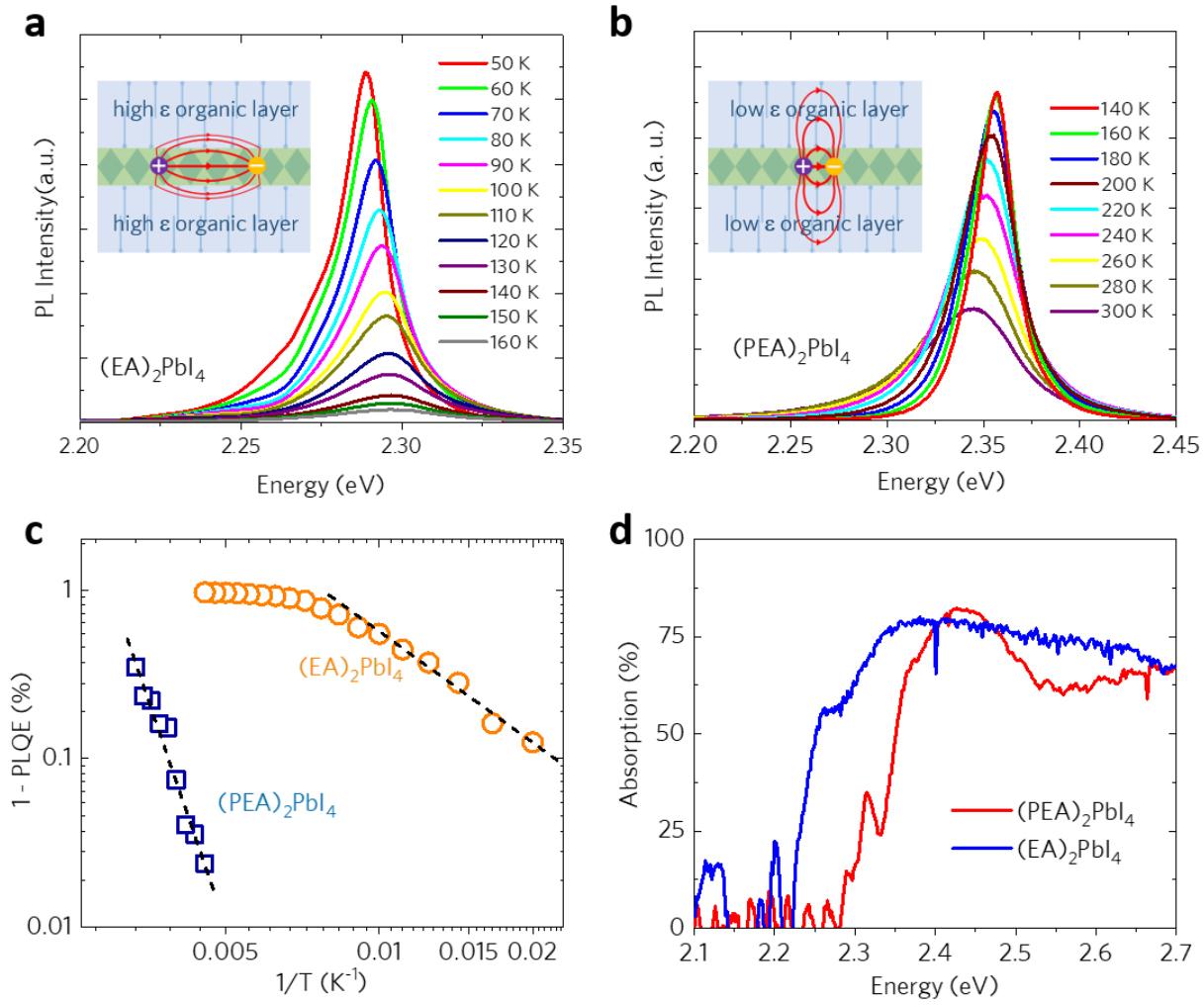
a
high ε organic layer
high ε organic layer
(EA)2PbI4
PL Intensity(a.u.)
Energy (eV)
50 K
60 K
70 K
80 K
90 K
100 K
110 K
120 K
130 K
140 K
150 K
160 K
b
low ε organic layer
low ε organic layer
(PEA)2PbI4
PL Intensity (a. u.)
Energy (eV)
140 K
160 K
180 K
200 K
220 K
240 K
260 K
280 K
300 K
c
(EA)2PbI4
(PEA)2PbI4
1 - PLQE (%)
1/T (K-1)
d
(PEA)2PbI4
(EA)2PbI4
Absorption (%)
Energy (eV)

Figure 2

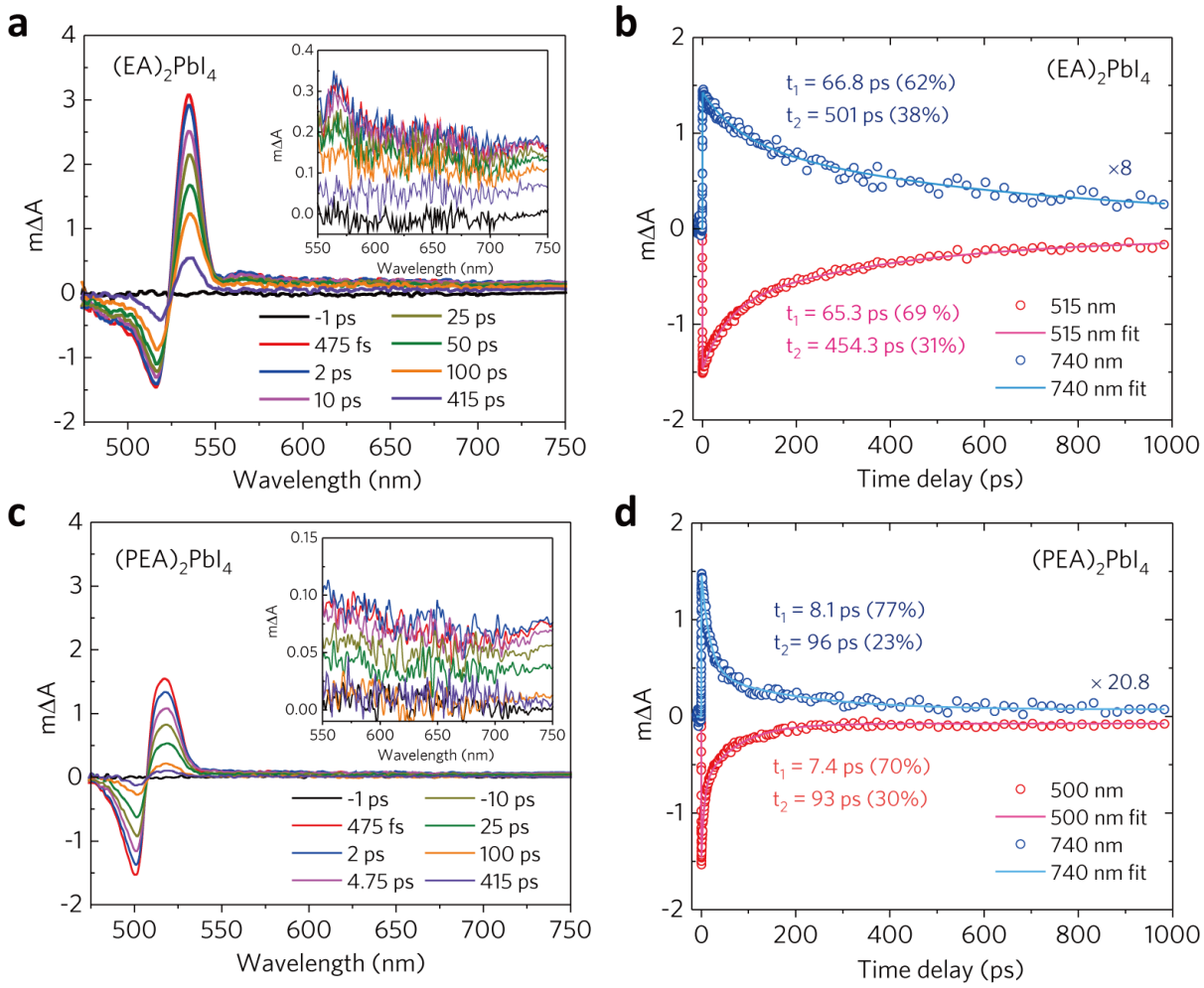
a
(EA)2PbI4
mΔA
Wavelength (nm)
-1 ps
475 fs
2 ps
10 ps
25 ps
50 ps
100 ps
415 ps
b
(EA)2PbI4
t1 = 66.8 ps (62%)
t2 = 501 ps (38%)
×8
t1 = 65.3 ps (69 %)
t2 = 454.3 ps (31%)
515 nm
515 nm fit
740 nm
740 nm fit
Time delay (ps)
c
(PEA)2PbI4
mΔA
Wavelength (nm)
-1 ps
475 fs
2 ps
4.75 ps
-10 ps
25 ps
100 ps
415 ps
d
(PEA)2PbI4
t1 = 8.1 ps (77%)
t2= 96 ps (23%)
× 20.8
t1 = 7.4 ps (70%)
t2 = 93 ps (30%)
500 nm
500 nm fit
740 nm
740 nm fit
Time delay (ps)

Figure 3

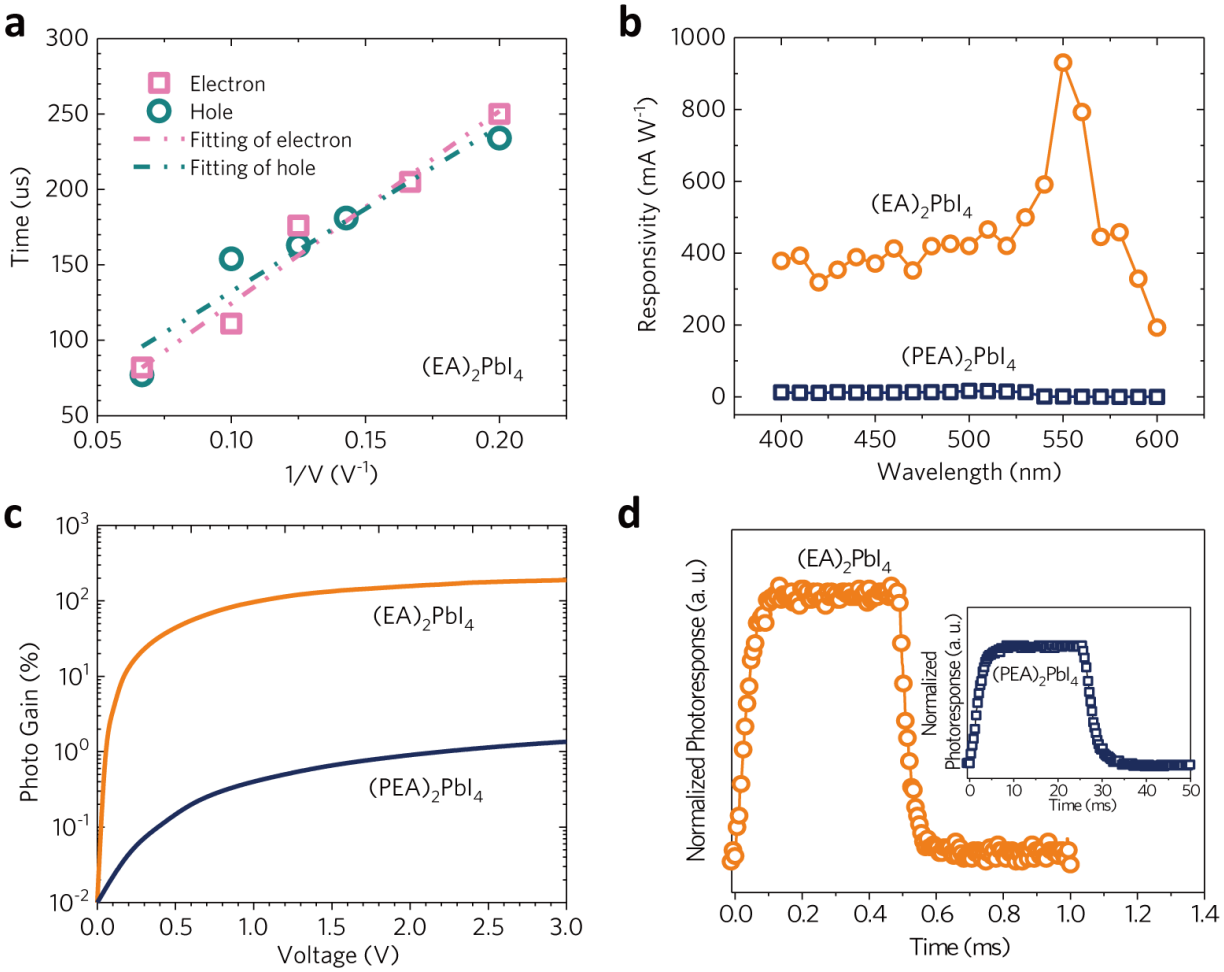
a
Electron
Hole
Fitting of electron
Fitting of hole
(EA)2PbI4
Time (us)
1/V (V-1)
b
(EA)2PbI4
(PEA)2PbI4
Responsivity (mA W-1)
Wavelength (nm)
c
(EA)2PbI4
(PEA)2PbI4
Photo Gain (%)
Voltage (V)
d
(EA)2PbI4
(PEA)2PbI4
Normalized Photoresponse (a. u.)
Time (ms)

Figure 4

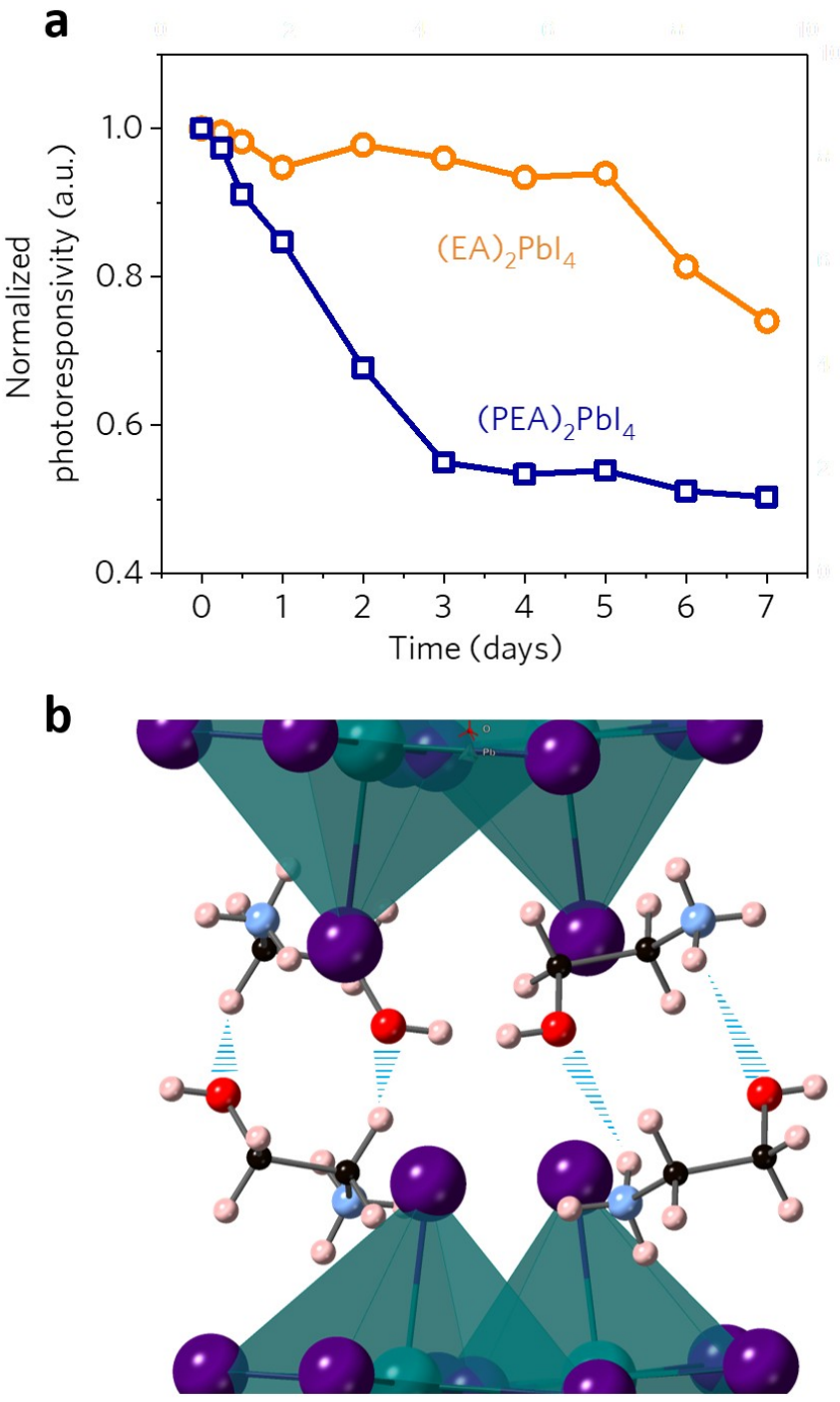
a
Normalized photoresponsivity (a.u.)
1.0
0.8
0.6
0.4
0
1
2
3
4
5
6
7
Time (days)
(EA)2PbI4
(PEA)2PbI4
b

Figure 5

Acknowledgements

This work was financially supported by the King Abdullah University of Science and Technology (KAUST) Office of Sponsored Research (OSR-2016-CRG5-3005), KAUST solar center (FCC/1/3079-08-01) and KAUST baseline funding.

Author Contributions

B.C., T.Y.L., and J.H.H. conceived the idea. B.C. calculated the exciton binding energy. T.Y.L. synthesized the materials and fabricated the MSM junctions. T.Y.L., B.C., K.T.H., R.Z.L, and C.H.L. designed and performed the optoelectronic and electrical measurements. I.A.A. and I.S.R. performed optical spectroscopy measurements. P.M. and O.F.M. designed and performed the femtosecond transient absorption measurements. X.H.M. and T.Y.L. arranged and analyzed the XRD experimental data. D.H.L. and A.J. did the absorption measurement. T.Y.L., N.D., and S.D. arranged and analyzed the synchrotron XPS experimental data. J.Y. and O.F.M. calculated the band structure. B.C., T.Y.L., P.C.W. and J.H.H analyzed the data and wrote the paper. All authors discussed the results and commented on the manuscript.

References and notes

1 Smith, I. C., Hoke, E. T., Solis-Ibarra, D., McGehee, M. D. & Karunadasa, H. I. A layered hybrid perovskite solar-cell absorber with enhanced moisture stability. *Angewandte Chemie* **126**, 11414-11417 (2014).

2 Tsai, H. *et al.* High-efficiency two-dimensional Ruddlesden–Popper perovskite solar cells. *Nature* **536**, 312-316 (2016).

3 Dohner, E. R., Jaffe, A., Bradshaw, L. R. & Karunadasa, H. I. Intrinsic white-light emission from layered hybrid perovskites. *Journal of the American Chemical Society* **136**, 13154-13157 (2014).

4 Dou, L. *et al.* Atomically thin two-dimensional organic-inorganic hybrid perovskites. *Science* **349**, 1518-1521 (2015).

5 Ma, D. *et al.* Single-crystal microplates of two-dimensional organic–inorganic lead halide layered perovskites for optoelectronics. *Nano Research* **10**, 2117-2129 (2017).

6 Yang, W. S. *et al.* High-performance photovoltaic perovskite layers fabricated through intramolecular exchange. *Science* **348**, 1234-1237 (2015).

7 Lee, M. M. e. a. Efficient hybrid solar cells based on meso-superstructured organometal halide perovskites. *Science* **338**, 643-647 (2012).

8 Burschka, J. *et al.* Sequential deposition as a route to high-performance perovskite-sensitized solar cells. *Nature* **499**, 316 (2013).

9 Jeon, N. J. e. a. Compositional engineering of perovskite materials for high-performance solar cells. *Nature* **517**, 476-480 (2015).

10 Zhou, H. *et al.* Interface engineering of highly efficient perovskite solar cells. *Science* **345**, 542-546 (2014).

11 Yang, S. *et al.* Ultrathin Two-Dimensional Organic–Inorganic Hybrid Perovskite Nanosheets with Bright, Tunable Photoluminescence and High Stability. *Angewandte Chemie International Edition* **56**, 4252-4255 (2017).

12 Yaffe, O. *et al.* Excitons in ultrathin organic-inorganic perovskite crystals. *Physical Review B* **92**, 045414 (2015).

13 Hanamura, E., Nagaosa, N., Kumagai, M. & Takagahara, T. Quantum wells with enhanced exciton effects and optical non-linearity. *Materials Science and Engineering: B* **1**, 255-258 (1988).

14 Hong, X., Ishihara, T. & Nurmikko, A. Dielectric confinement effect on excitons in PbI 4-based layered semiconductors. *Physical Review B* **45**, 6961 (1992).

15 Ishihara, T., Takahashi, J. & Goto, T. Exciton state in two-dimensional perovskite semiconductor (C10H21NH3) 2PbI4. *Solid state communications* **69**, 933-936 (1989).

16 Pedesseau, L. *et al.* Advances and promises of layered halide hybrid perovskite semiconductors. (2016).

17 Milot, R. L. *et al.* Charge-carrier dynamics in 2D hybrid metal–halide perovskites. *Nano Lett* **16**, 7001-7007 (2016).

18 Blancon, J.-C. *et al.* Extremely efficient internal exciton dissociation through edge states in layered 2D perovskites. *Science*, eaal4211 (2017).
19 Smith, M. D. *et al.* Decreasing the electronic confinement in layered perovskites through intercalation. *Chemical Science* **8**, 1960-1968 (2017).
20 Mercier, N., Poiroux, S., Riou, A. & Batail, P. Unique hydrogen bonding correlating with a reduced band gap and phase transition in the hybrid perovskites (HO (CH2) 2NH3) 2PbX4 (X= I, Br). *Inorganic chemistry* **43**, 8361-8366 (2004).
21 Covington, A. *Physical chemistry of organic solvent systems*. (Springer Science & Business Media, 2012).
22 Kagan, C., Mitzi, D. & Dimitrakopoulos, C. Organic-inorganic hybrid materials as semiconducting channels in thin-film field-effect transistors. *Science* **286**, 945-947 (1999).
23 Mitzi, D. B. *et al.* Hybrid field-effect transistor based on a low-temperature melt-processed channel layer. *Advanced Materials* **14**, 1772-1776 (2002).
24 Savenije, T. J. *et al.* Thermally activated exciton dissociation and recombination control the carrier dynamics in organometal halide perovskite. *The journal of physical chemistry letters* **5**, 2189-2194 (2014).
25 Begum, R. *et al.* Engineering Interfacial Charge Transfer in CsPbBr3 Perovskite Nanocrystals by Heterovalent Doping. *Journal of the American Chemical Society* **139**, 731-737 (2016).
26 Zhang, Y. *et al.* Direct-Indirect Nature of the Bandgap in Lead-Free Perovskite Nanocrystals. *The Journal of Physical Chemistry Letters* **8**, 3173-3177 (2017).
27 Shi, D. *et al.* Low trap-state density and long carrier diffusion in organolead trihalide perovskite single crystals. *Science* **347**, 519-522 (2015).
28 Ma, N. & Jena, D. Charge scattering and mobility in atomically thin semiconductors. *Physical Review X* **4**, 011043 (2014).
29 Konstantatos, G. *et al.* Ultrasensitive solution-cast quantum dot photodetectors. *nature* **442**, 180 (2006).
30 Lopez-Sanchez, O., Lembke, D., Kayci, M., Radenovic, A. & Kis, A. Ultrasensitive photodetectors based on monolayer MoS2. *Nature nanotechnology* **8**, 497-501 (2013).
31 Li, D., et al. Electronic and ionic transport dynamics in organolead halide perovskites. *ACS nano* **10**, 6933-6941 (2016).